Published in final edited form as:
Nature. 2019 May ; 569(7754): 136–140. doi:10.1038/s41586-019-1115-5.

Mammalian ISWI and SWI/SNF selectively mediate binding of distinct transcription factors

Darko Barisic[#1,2,4], **Michael B. Stadler**[#1,3], **Mario Iurlaro**[#1], and **Dirk Schübeler**[1,2,†]

[1]Friedrich Miescher Institute for Biomedical Research, Basel, Switzerland [2]Faculty of Science, University of Basel, Basel, Switzerland [3]Swiss Institute of Bioinformatics, Basel, Switzerland

[#] These authors contributed equally to this work.

Abstract

Chromatin remodeling complexes evict, slide, insert or replace nucleosomes, which represent an intrinsic barrier for access to DNA. Remodelers function in most aspects of genome utilization including transcription factor (TF) binding, DNA replication and repair1,2. While they are frequently mutated in cancer3, it remains largely unclear how the four mammalian remodeler families (SWI/SNF, ISWI, CHD and INO80) orchestrate the global organization of nucleosomes. To gain insight into this matter, we generated viable embryonic stem cells that lack Snf2h, the ATPase of ISWI complexes, enabling to study its cellular function and contrast it to Brg1, the ATPase of SWI/SNF. Loss of Snf2h decreases nucleosomal phasing and increases linker lengths providing *in vivo* evidence for ISWI function in ruling nucleosomal spacing in mammals. Systematic analysis of transcription factor binding reveals their selective requirement on either remodeling activity. One group critically depends on Brg1 and contains the transcriptional repressor REST, while a non-overlapping set relies on Snf2h and includes the insulator protein CTCF. This selectivity readily explains why chromosomal folding and insulation of topologically associated domains requires Snf2h, but not Brg1.

Collectively, this study shows that mammalian ISWI is critical for nucleosomal periodicity and nuclear organization and that transcription factors rely on specific remodeling pathways for proper genomic binding.

Deletion of Brg1, the essential ATPase subunit of the SWI/SNF family4,5, decreases binding of pluripotency transcription factors such as Oct4, Sox2 and Nanog4,6,7, arguing for a function of SWI/SNF in TF binding in line with its ability to eject nucleosomes *in vitro*2,8,9.

[†]Correspondence and requests for materials should be addressed to Dirk Schübeler (dirk.schubeler@fmi.ch).
[4]current address: Weill Cornell Medicine, New York, USA

The authors declare no competing interests.

Authors Contribution

DB, MI, MBS and DS conceived and planned the experiments. DB, MI executed the experiments and contributed to initial data analysis. MBS performed comprehensive computational data analysis. DS supervised the project. All authors contributed to interpretation of the results and writing of the manuscript.

The *in vivo* role of the ISWI family is less clear. ISWI complexes use two catalytic subunits, SNF2H and SNF2L. SNF2H forms five remodeler complexes in mammals; ACF, CHRAC, NoRC, WICH and RSF2,10. They do not eject nucleosomes but slide them along DNA *in vitro*11–13, leading to a model of a 'ruler' function that confers defined linker-length14,15. Notably, transient knockdown of Snf2h in HeLa cells causes reduced nucleosomal positioning around CTCF binding sites16.

While Snf2h deletion is embryonically lethal in mice and derived ES cells17, we were able to generate ES clones with homozygous frameshift mutation in exon 6 of the *Smarca5/Snf2h* gene using CRISPR/Cas9 and resulting absence of SNF2H protein (Figure 1a,b and Extended Data Fig. 1a) enabling to study the role of ISWI chromatin remodelers in a cellular context. Snf2h knockout (Snf2h ko) cells show normal morphology, largely unchanged cell cycle profile and are able to form ES colonies (Fig. 1a, Extended Data Figure 1b,c).

To test if observed phenotypes result from absence of SNF2H catalytic activity, we reintroduced into the knockout background the wildtype SNF2H ("add-back wildtype") protein and an isoform containing a point mutation in the ATP-binding domain ("add-back mutant"), which abolishes ATPase activity yet keeps SNF2H-containing complexes intact18 (Fig.1b). Wildtype add-back reverted cell proliferation to wildtype levels (~13% increase; Extended Data Fig. 1d). Transcriptome analysis identified almost 2000 differentially expressed genes upon loss of Snf2h (FDR < 0.05, Fig. 1c and Extended Data Fig. 1f), which are enriched for developmental and proliferative functions (Extended Data Fig. 1g). Importantly the wildtype add-back completely reverts all gene expression changes illustrating that these do not result from accumulated DNA damage, loss of an epigenetic memory or spontaneous differentiation (Fig. 1c and Extended Data Fig. 1h). Strikingly, Snf2h ko and add-back mutant cells appear almost identical at the transcriptional level demonstrating that mis-regulation is caused by the absence of catalytic activity and not by complex disassembly and thus potentially indirect. It further argues against a role for SNF2L in compensating for absence of SNF2H19.

Snf2h ko cells show ES cell characteristics and properly express pluripotency markers yet fail to form proper embryoid bodies and neuronal progenitors (Extended Data Fig. 1e,f). Taken together, loss of the catalytic activity of Snf2h in mES cells leads to global changes in transcription, reduced proliferation and differentiation potential.

To determine potential contribution of Snf2h to nucleosome patterns we sequenced mononucleosomal fragments generated by MNase digestion at a depth sufficient to locally score positioning (see Methods). Visual inspection reveals local reduction which can be quantified by inferring nucleosome phasing through Fourier transformation (Fig. 1d,e and Extended Data Fig. 2). Overlaying phasing profiles reveals limited effects around transcriptional start sites (TSS) (Extended Data Fig. 3a-c), reminiscent of the yeast phenotype20 and knockdown in a human cancer cell line16. The opposite occurs at regulatory regions, where phasing is reduced several-fold yet fully reversed by wildtype protein (Fig. 1f and Extended Data Fig. 3d).

Since DNA methyltransferases preferentially methylate linker DNA, phasing is also evident in patterns of endogenous DNA methylation21. Bisulfite sequencing reveals that this periodicity is reduced upon loss of Snf2h (Fig. 1g and Extended Data Fig. 4) validating by a cell-intrinsic measure that absence of Snf2h decreases nucleosome phasing.

Since SNF2H generates equally spaced nucleosomal arrays *in vitro*2 we asked if this “ruler” function operates in mammalian cells. We determined the nucleosomal repeat length (NRL) in wildtype, mutant and rescue clones by performing ATAC-seq. This transposase insertion assay identifies open regulatory regions22 but also creates fragments corresponding to mono-, di- and tri-nucleosomes22 (Extended Data Fig. 5a,b). These enable to infer the nucleosome repeat length revealing an increase of ~9 base pairs in absence of Snf2h, which is reverted by wt but not catalytically inactive add-back (Fig. 2a). To test if this is specific to Snf2h, we performed the same analysis in cells lacking Brg1, the ATPase subunit of the SWI/SNF remodeler complexes, utilizing a cell line enabling inducible deletion of Brg123. This reveals that NRL does not change significantly in absence of Brg1 using our (Fig. 2a) or published datasets (Extended Data Fig. 5c). Consequently, increase of NRL is specific for loss of ISWI.

To challenge this finding we also calculated NRL from same-strand alignment distances of our MNase data24,25 (Extended Data Fig. 6), revealing a comparable increase in NRL upon loss of Snf2h (Fig. 2b,c). This is readily reverted by reintroduction of functional SNF2H (Fig. 2b,c). Analysis of published MNase data from Brg1-deleted cells confirms that this NRL increase is ISWI-specific (Extended Data Fig. 5d,e). Thus, loss of SNF2H activity causes a global NRL increase providing *in vivo* evidence for the predicted ruler function which appears specific for ISWI.

To examine if chromatin remodelers affect TF binding, we determined changes in the regulatory landscape upon their deletion using ATAC-seq (Extended Data Fig. 7). More specifically we screened genomic regions that changed accessibility upon deletion of Snf2h or Brg1 for motifs of 519 mammalian transcription factors with known sequence preferences26 (Fig. 3a and Extended Data Fig. 8a-b). This exposed two non-overlapping sets of factors whose binding appears dependent on Snf2h or Brg1 activity, respectively. Remarkably, specific transcription factors are dependent on ISWI activity but are unaffected by loss of SWI/SNF, and vice versa. This suggests a striking specificity compatible with a model where interactions between transcription factors and particular nucleosome remodelers are fundamental for transcription factor binding to their cognate motifs.

To further explore this model, we focused on two Zinc-finger transcription factors with asymmetric binding responses to loss of Snf2h or Brg1: CTCF and REST. Importantly both TFs utilize similar DNA binding domains and recognize large motifs of over 17bp with high specificity27,28. The ATAC-seq profile over CTCF sites is virtually unchanged upon Brg1 deletion, with nucleosome phasing adjacent to bound sites, a signal that is largely absent in Snf2h knockout cells (Extended Data Fig. 8e). This suggests that CTCF depends on Snf2h but not Brg1 for binding.

Conversely, a mirrored situation is evident at REST sites, where phasing is unaffected in Snf2h ko cells yet severely altered in the absence of Brg1 (Extended Data Fig. 8f). This is similarly evident in MNase profiles as phasing of nucleosomes flanking CTCF motifs is diminished in the absence of Snf2h, as shown previously16, with concomitant increase of nucleosome occupancy over the motif (Fig. 3b). This is readily reversed by re-expression of wild-type SNF2H (Fig. 3b) and not caused by decreased CTCF levels (Extended Data Fig. 8g). Cellular DNA methylation confirms this reduced phasing (Extended Data Fig. 8h). In contrast, phasing at REST sites is unaffected in Snf2h ko, yet spacing increases notably (Fig. 3c). This is in line with the NRL increase, which importantly is also visible at the level of DNA methylation (Extended Data Fig. 8i,j). Experimental measurement of TF binding by ChIP-seq reveals no effect on genomic binding of REST in the ISWI mutant but genome-wide reduction of CTCF binding at its cognate motifs, in line with previous observations upon knockdown of Snf2h in a human cell line16 (Fig. 3d,e and Extended Data Fig. 9). Re-expression of wt SNF2H, but not of inactive mutant, fully restores CTCF binding (Extended Data Fig. 9). Importantly, opposing patterns are detected in the Brg1 ko, where REST binding is strongly reduced, while CTCF binding is unaffected (Figure 3d,e and Extended Data Fig. 9). Thus genome-wide binding fully validates predictions based on differential local accessibility, confirming that both TFs critically rely on distinct remodeler machineries for binding.

The degree of binding reduction of REST and CTCF is locus-specific as some sites are more dependent on the respective remodeler for binding than others (Extended Data Fig. 10a,c). For both TFs strongly dependent sites tend to lie distal to genes and not in areas of high overall accessibility (Extended Data Fig. 10b,d).

CTCF is essential for long-range chromosome looping via interaction with cohesin (reviewed in29,30), which is critical for gene regulation. One might expect that loss of Snf2h would not affect chromosomal loops since over 95% of CTCF protein needed to be depleted to affect chromosome conformation31. In contrast, CTCF protein levels are unaffected and binding still detectable at many sites in Snf2h ko (Extended Data Figs. 8g and 10). We nevertheless performed Hi-C in Brg1 and Snf2h mutants and matching wildtype cells. Lack of Snf2h affects formation of chromatin loops and insulation of topologically associating domains (TADs) as is evident from contact maps (Fig. 4a and Extended Data Fig. 11a). In contrast, deletion of Brg1, which does not cause any change in CTCF binding, reveals a largely unchanged TAD profile, arguing for a Snf2h-specific phenotype (Fig. 4b and Extended Data Fig. 11b). This is confirmed by hierarchical clustering of all Hi-C datasets, showing Brg1 ko clustering with wildtype, while Snf2h ko clusters separately (Fig. 4c).

To quantify this effect we calculated insulation scores32 at all TAD boundaries containing CTCF sites. As suggested by visual inspection, loss of Snf2h reduces insulation at TAD boundaries across all chromosomes, while Brg1 had no effect (Fig. 4d and Extended Data Fig. 11c). Notably the severity of this loss resembles the one measured upon almost complete loss of CTCF in the same cell type31.

To investigate potential effects on chromatin loop formation, we measured contact frequencies at CTCF and cohesin-bound loops, as identified by HiChIP of a central

component of the cohesin complex, Smc1a33. This revealed significant reduction of interactions, showing an integral role of Snf2h in the formation and maintenance of chromatin loop domains. This function is again ISWI-specific, as loss of Brg1 had no effect (Fig. 4e and Extended Data Fig. 12a-d) and was most pronounced at convergent CTCF sites with strong dependency on Snf2h (Extended Data Fig. 12e). Finally, similar to CTCF degradation, both remodeler deletions do not impair higher-order interactions of active and passive chromosome domains into the so-called A/B compartments31,34 (and Extended Data Fig. 12f,g). We conclude that Snf2h plays a crucial role in chromatin architecture and TAD formation likely through its requirement for CTCF binding. This links ISWI but not SWI/SNF remodeler activity to nuclear organization.

In summary absence of Snf2h causes a global increase in linker length and reduced nucleosomal phasing showing *in vivo* ruler activity of ISWI in mammals. This appears species specific since deletion of ISWI function in yeast and Drosophila causes shortening of the linker length15,35. It is further remodeler specific as Brg1 depletion does not cause NRL changes.

Our finding that a class of transcription factors depends on ISWI suggests that nucleosomal sliding contributes to TF binding. While the exact mechanism remains open, one scenario could be that ISWI, in the process of creating ordered arrays, repositions a nucleosome that blocks a previously occupied binding motif. In line with this, absence of ISWI leads to increased nucleosomal abundance over binding sites with reduced TF occupancy. Irrespective of the exact mechanism it is clearly distinct to that of Brg1 since dependent TFs do not overlap, even though factors such as REST and CTCF share molecular similarities in binding domains and motif length. This pathway-specific behavior supports a model where remodelers enable TF binding by selective recruitment or specific chromatin requirements rather than by creating global nucleosome dynamics, which in turn create binding opportunities in a factor-independent fashion. As Snf2h constitutes the catalytic subunit of several ISWI complexes, it will be important to study whether these phenotypes are complex-specific or shared among the entirety of the ISWI family.

Thus far only CTCF itself, cohesin and cohesin-loading/release factors have been functionally linked to genome-wide nuclear topology30. ISWI affects CTCF binding without reducing its abundance, which nevertheless impacts TAD insulation similarly to degradation of CTCF itself. This adds a chromatin remodeler enzyme as critical for nuclear organization and proper TAD insulation, illustrating how this class of proteins is involved in many DNA templated events, including the three-dimensional organization of the genome.

Extended Data

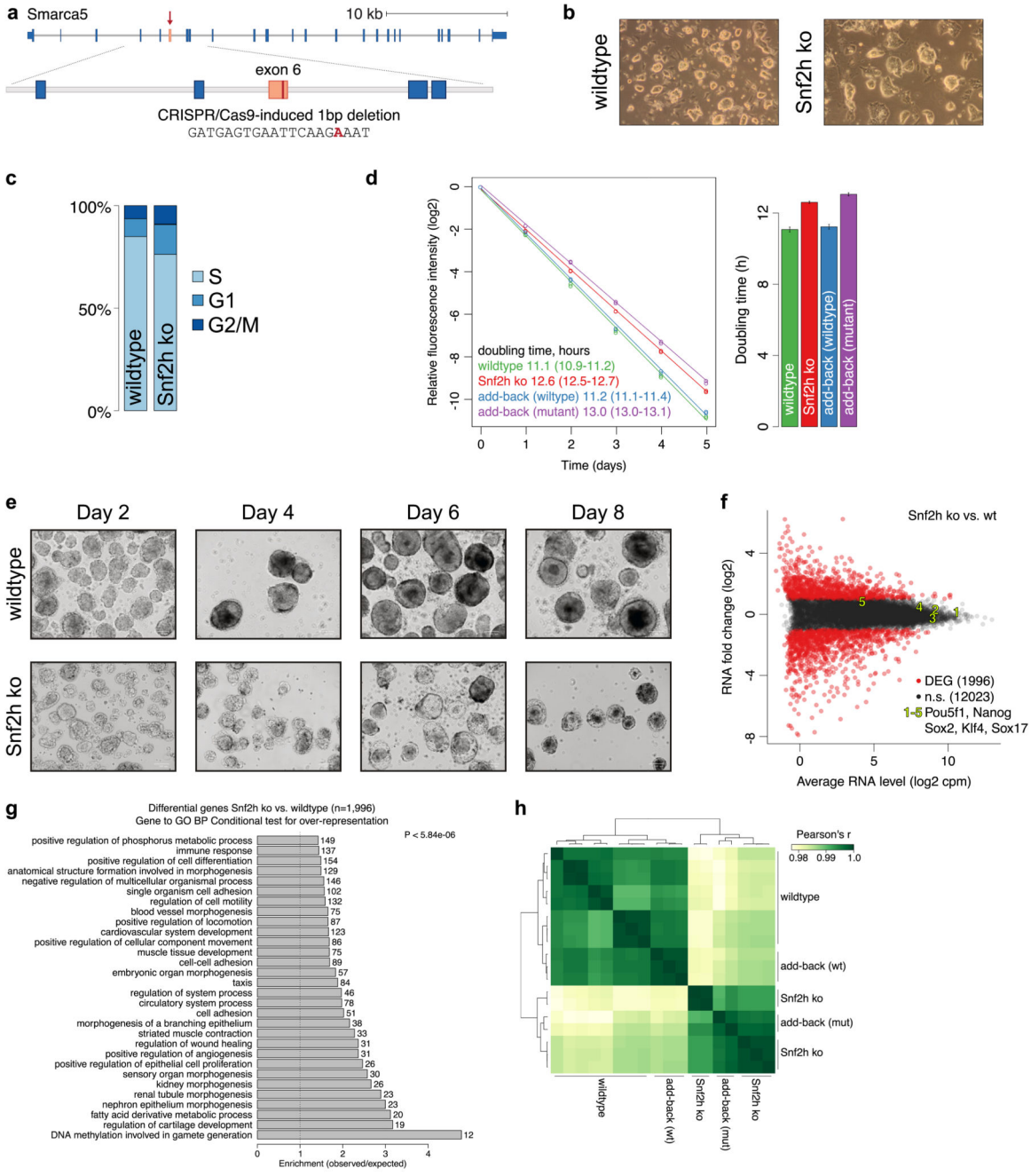

Extended Data Figure 1. Phenotype description of Snf2h ko mouse ES cells.

a, Generation of Snf2h ko mouse embryonic cell lines. **b,** Images of wildtype and Snf2h ko cell cultures grown on gelatin-coated plates. **c,** Cell cycle phase composition, measured by FACS (DNA content and BrdU incorporation). **d,** Cell cycle duration estimated by exponential loss of fluorescence dye. Doubling time was estimated from the slope of a linear fit to the data and is indicated (95% confidence intervals in parentheses). **e,** Images of wildtype and Snf2h ko cells during embryoid body formation. **f**, Differentially expressed genes between Snf2h ko and wildtype cells. Pluripotency marker genes are unchanged

Europe PMC Funders Author Manuscripts

(labelled as 1 to 5). **g**, Gene ontology (GO) terms enriched in the set of differentially expressed genes between Snf2h ko and wt ES cells. The bars are the observed/expected ratios for the 30 most significant terms from the “Biological Process” section, with the number of differentially expressed genes associated to a term shown on the right. All reported GO terms have P values of 5.84e-06 or smaller. All genes with an FDR < 0.05 and an absolute fold-change > 2.0 were used (n=1,996), and terms with less than 5 or more than 1,000 associated genes were filtered out. **h**, Correlation-based clustering of RNA-seq profiles, illustrating that the transcriptome of wildtype add-back cells closely resembles the one of wildtype cells, while mutant add-back cells are still grouped with Snf2h ko cells.

Europe PMC Funders Author Manuscripts

Europe PMC Funders Author Manuscripts

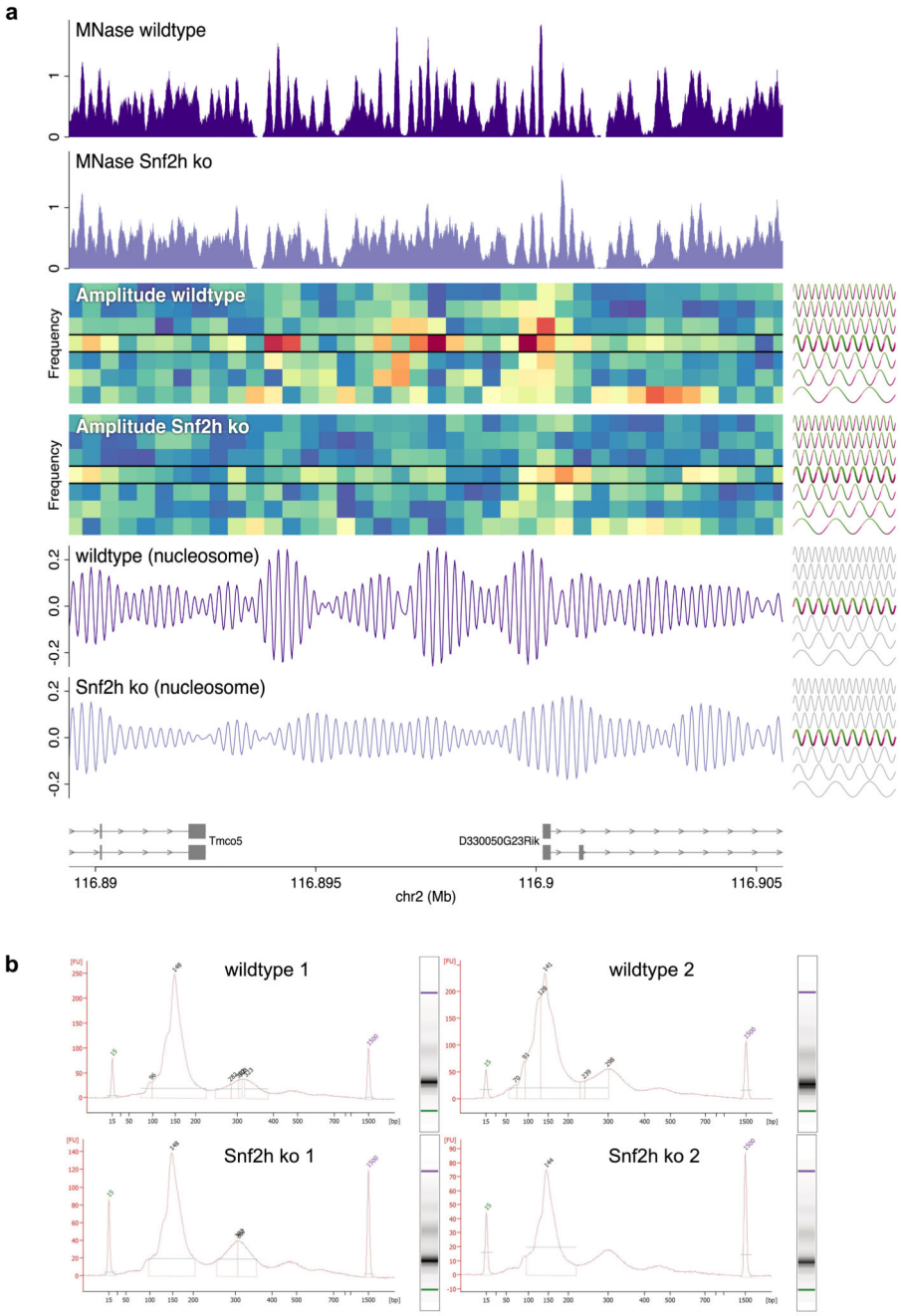

Extended Data Figure 2. Local quantification of nucleosome phasing using MNase-seq data.

a, Locus on chromosome 2 showing MNase-seq read densities, amplitudes for different frequencies (periods of 764, 382, 255, 191, 153, 127 and 109 bp) and reconstructed signal using only the nucleosome frequency (191 bp period). **b,** Bioanalyzer traces of MNase digests used for MNase-seq experiments.

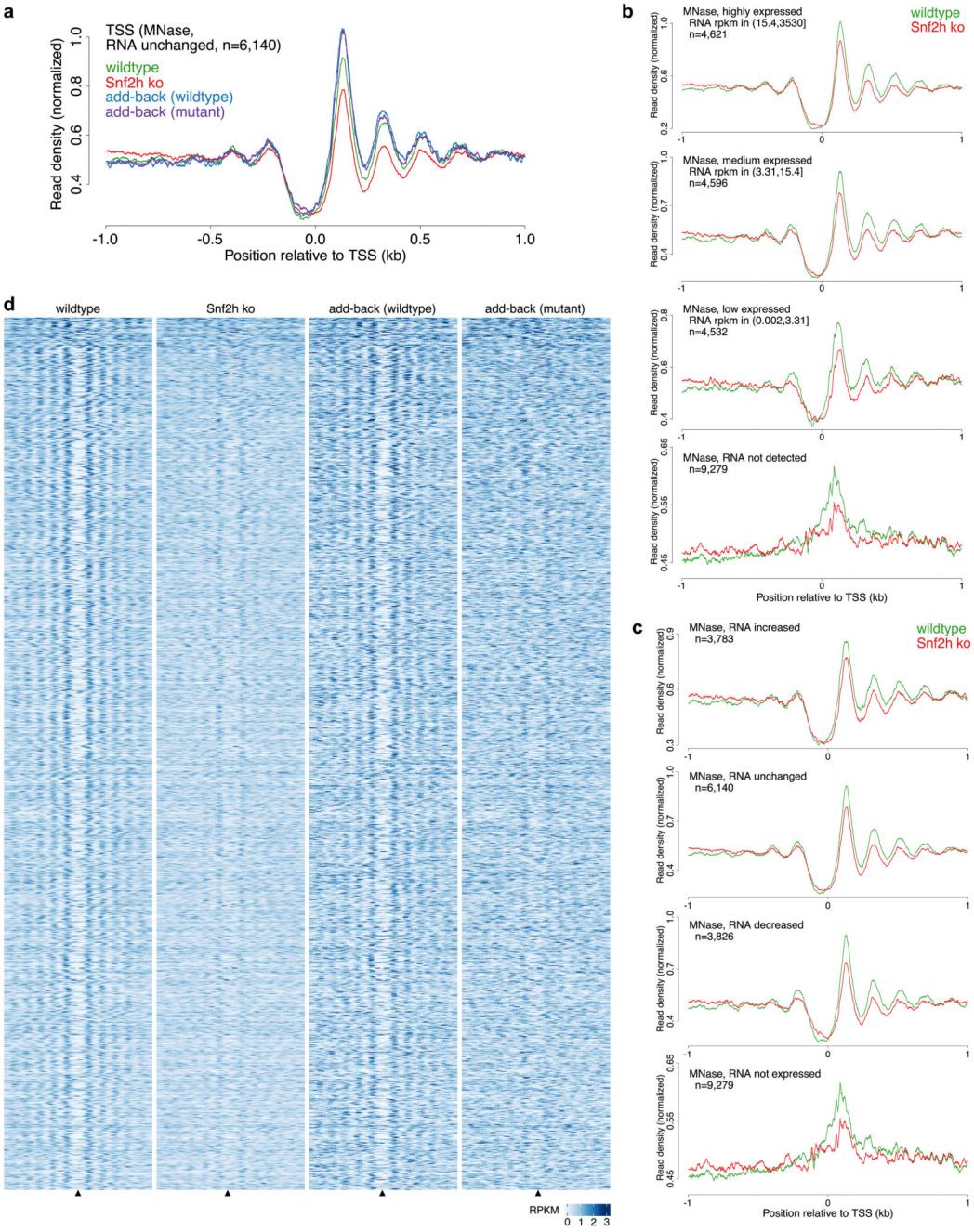

Extended Data Figure 3. MNase read densities around TSS and DHS.

a, Average MNase read densities around transcript start sites (TSS). **b**, Average MNase read densities around transcript start sites (TSS), from top to bottom for genes with high, medium or low RNA levels or whose RNA is not detected in neither Snf2h ko nor wildtype, respectively. **c**, MNase read densities around TSS as in (b), from top to bottom for genes whose RNA levels increase, remain unchanged, decrease in Snf2h ko compared to wildtype, or whose RNA is not detected, respectively. **d**, MNase-seq alignment densities in a 2kb window around strong distal DHS. 5,000 regions with the highest 95th percentile values in

Europe PMC Funders Author Manuscripts

wildtype were selected from 55,201 regions in total, and aligned at the centre of the DHS (arrow at the bottom).

Europe PMC Funders Author Manuscripts

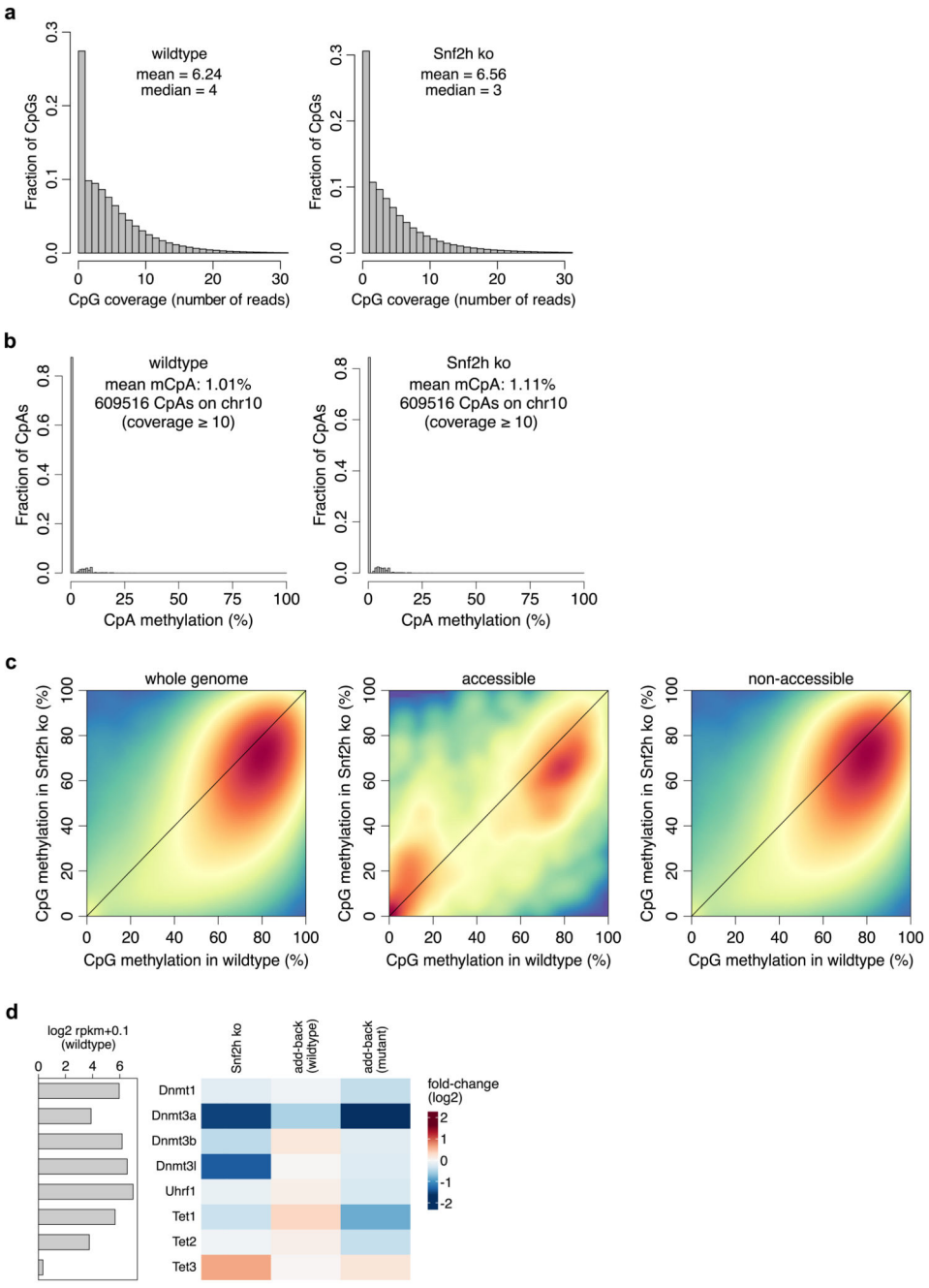

Extended Data Figure 4. Characterization of genome-wide DNA methylation in Snf2h ko and wt cells.

a, Distributions of CpG read coverage in whole-genome bisulfite sequencing DNA methylation analysis. **b,** Distribution of CpA methylation (chr10). **c,** 2D-densities comparing CpG methylation in wildtype and Snf2h ko across different domains of the genome. **d**, RNA levels and changes relative to wildtype of genes involved in DNA methylation.

Europe PMC Funders Author Manuscripts

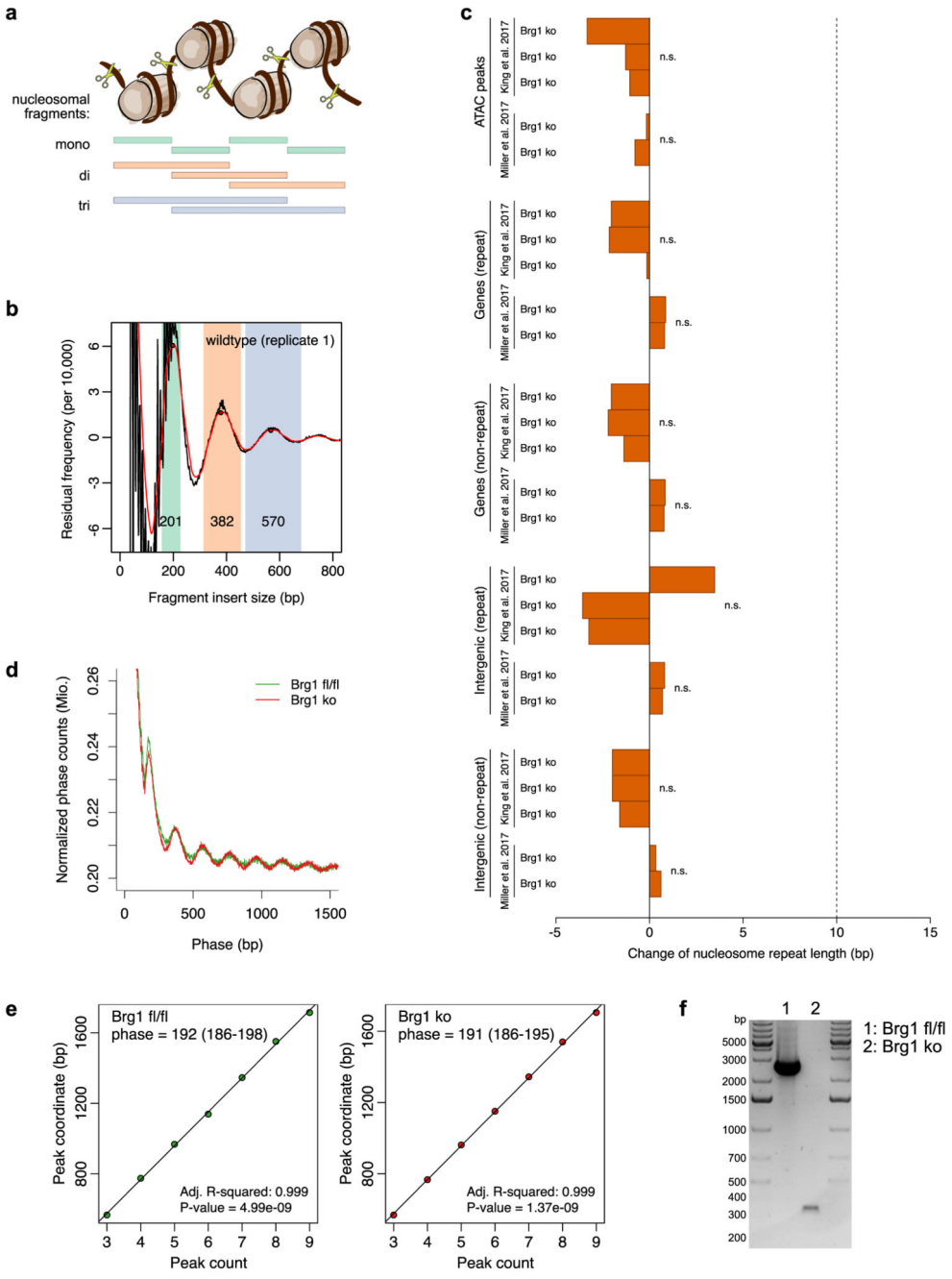

Extended Data Figure 5. NRL estimation in Brg1 conditional ko cells.

a, Scheme illustrating transposase insertion in chromatin. **b**, Mono-, di- and tri-nucleosomal fragment lengths estimated from smoothed and de-trended ATAC-seq fragment sizes (here showing wildtype replicate 1 as an example). The three estimates are averaged to obtain a single value per biological replicate. **c**, Estimated changes in nucleosome repeat lengths based on ATAC-seq data from Miller et al. 2017 and King et al. 2017 (as indicated) in Brg1 ko compared to controls. None of the datasets shows a significant increase of values (all P values > 0.05, one-sided Welch two sample t-test). **d,e,** MNase-based estimation of

Europe PMC Funders Author Manuscripts

nucleosome repeat length upon Brg1 deletion using data from Miller et al. 2017. e) Counts of distances between same-strand MNase-seq alignments (phase) in Brg1 fl/fl and Brg1 ko cells. e) Linear fits to the phase peaks from (d) and resulting nucleosome repeat lengths with 95% confidence intervals. **f,** Genotyping PCR for floxed (2507bp product) and deleted (313bp) Brg1 cells.

Europe PMC Funders Author Manuscripts

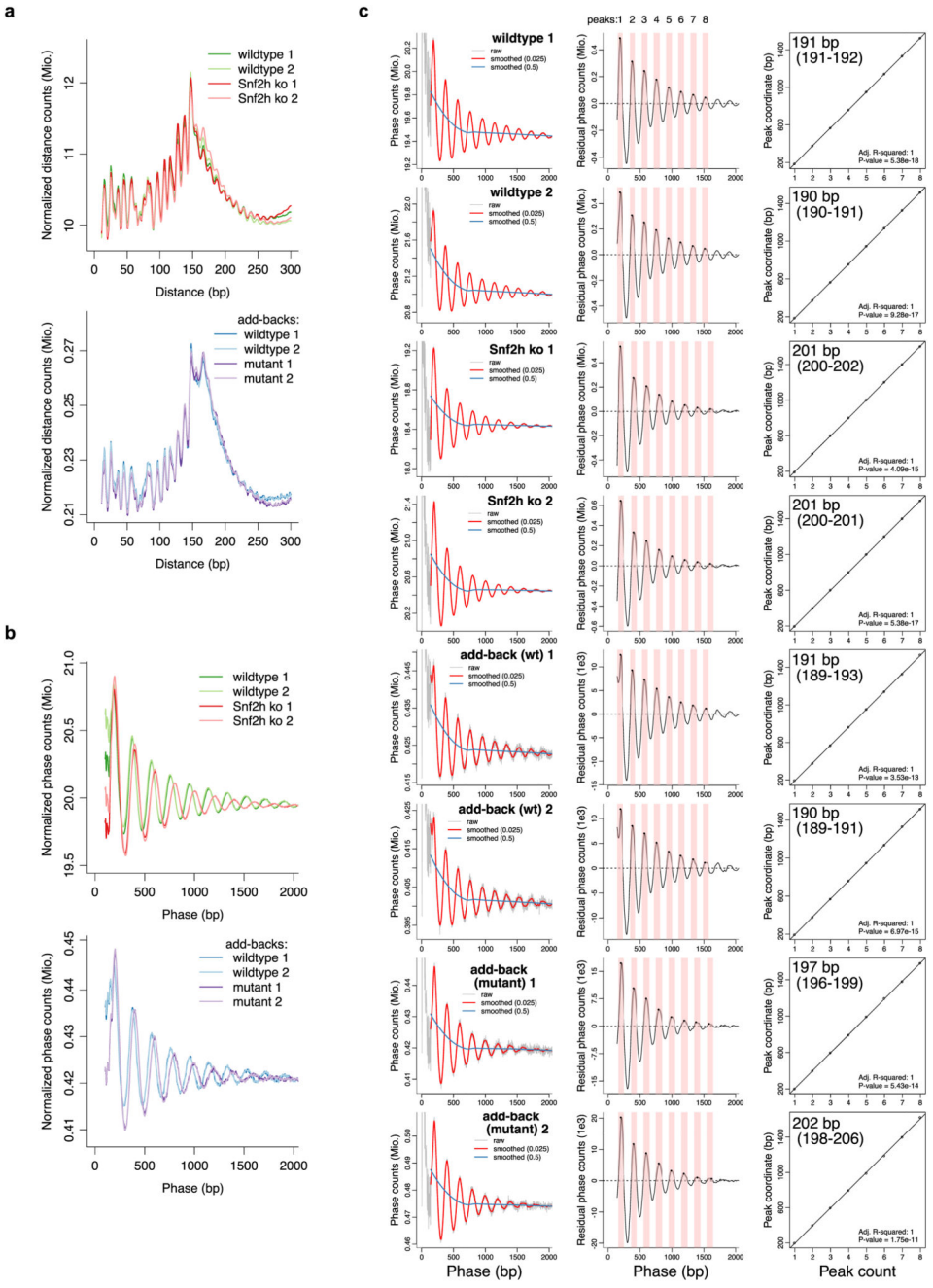

Extended Data Figure 6. NRL estimation in Snf2h ko and wt cells using MNase data.

a, Counts of opposite-strand MNase-seq alignment distances illustrating the average fragment length characteristic of a mono-nucleosome particle. **b,** Counts of same-strand MNase-seq alignment distances (phases). **c,** For each replicate MNase-seq dataset, counts of same-strand alignment distances (phases, left) with low- and high-span loess fits (red and blue, respectively), peak detection in residual phase counts (difference between low- and high-span fits, middle), and linear fits to the peak positions with nucleosome phase and 95%-confidence interval (right).

Europe PMC Funders Author Manuscripts

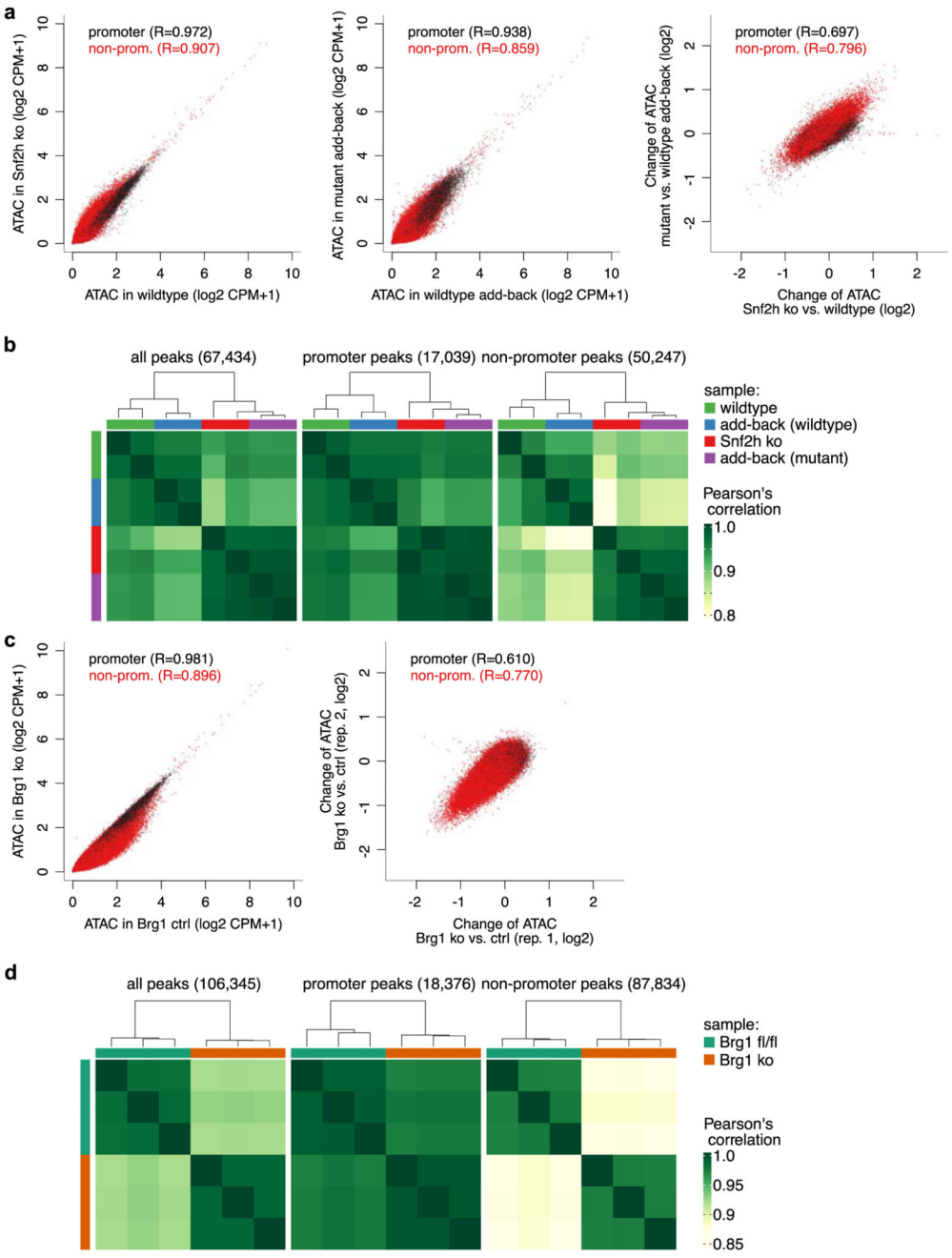

Extended Data Figure 7. Chromatin accessibility in Snf2h ko, Brg1 ko and control cells.

a, Scatter plots of absolute ATAC signal in promoter and non-promoter peaks (shown in black and red, respectively) of wildtype and Snf2h ko (left), wildtype and mutant add-back (middle), and corresponding changes of ATAC signal (right). R indicates Pearson's correlation coefficient. **b**, Pairwise correlation heatmaps for absolute ATAC signal in all, promoter and non-promoter peaks (left, middle and right) between wildtype, Snf2h ko and add-back samples (two replicates each). **c,d**, Same as in a) and b) for wildtype (Brg1 fl/fl) and Brg1 ko samples (three replicates each).

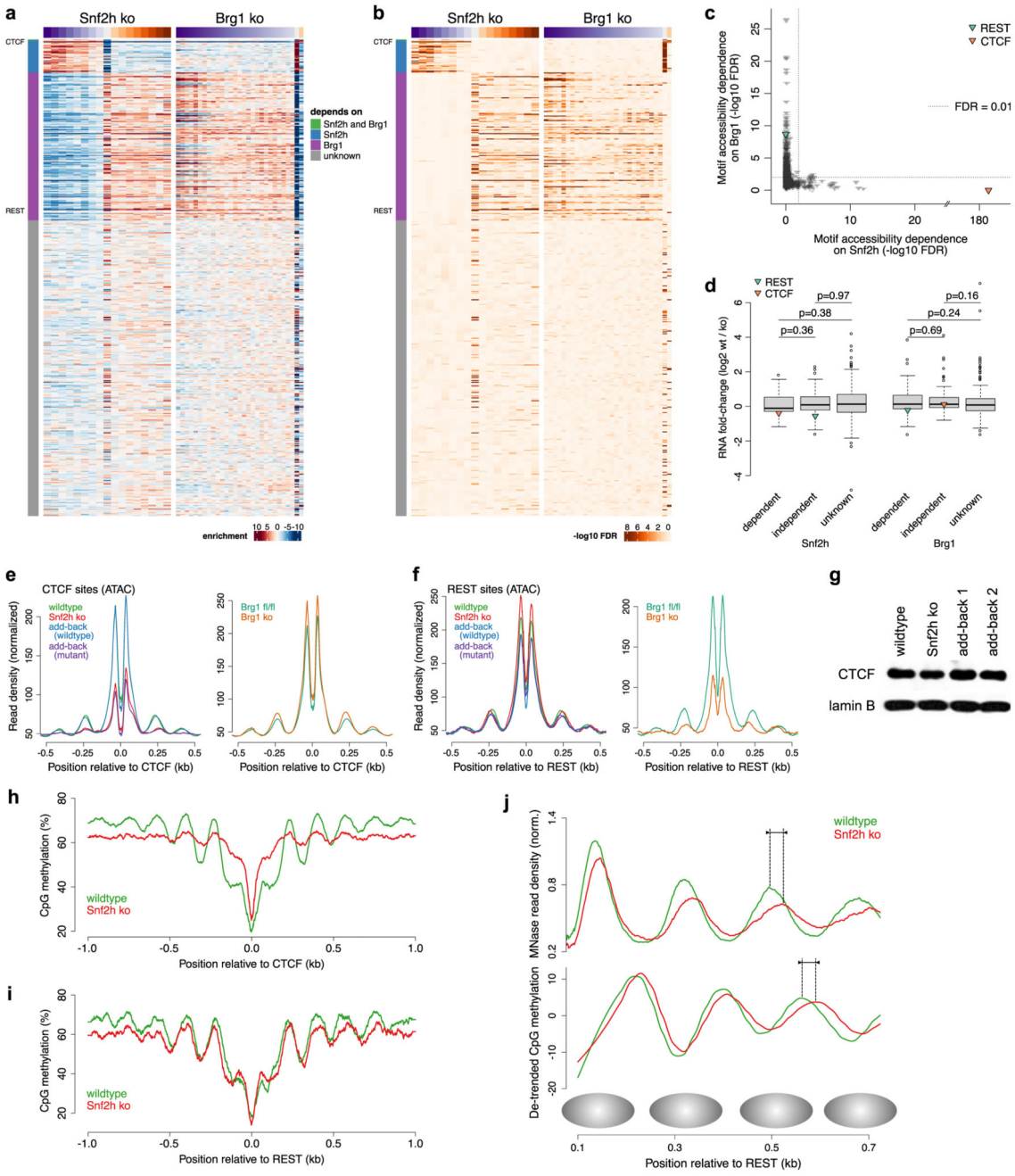

Extended Data Figure 8. Characterization of Snf2h- and Brg1-dependent transcription factors.

a,b, Enrichments of predicted TF sites in ATAC-seq peak bins compared to all other bins were calculated using HOMER and shown as Pearson residuals (a, (obs-exp)/√exp) or significance (b, -log10 FDR) for known motifs (rows) and bins of ATAC-seq peaks (columns). Peaks were binned into unchanged accessibility (change of less than 1.5-fold, gray), and bins of 1,500 peaks each with increasing or decreasing fold-changes (orange and purple). The colour bars on the left indicate the TF's dependency on chromatin remodelers (Snf2h and Brg1, Snf2h, Brg1 or unknown). **c,** Significance (log10 FDR) of motif

Europe PMC Funders Author Manuscripts

enrichment in the bin of peaks with the strongest decrease of accessibility, compared between Snf2h ko and Brg1 ko. Dashed lines indicate the significance thresholds used to classify TFs that depend on a given chromatin remodeller. **d,** RNA log2 fold-changes for TF genes with different dependency on chromatin remodelers. The “independent” class refers to TFs whose motifs are enriched in the bin with ATAC-seq peaks of unchanged accessibility. P values have been calculated using a two-sided Wilcoxon rank sum test with continuity correction. **e,f,** ATAC profiles around binding sites for transcription factors CTCF (e) and REST (f) with differing dependency on Snf2h or Brg1. **g,** Western blot showing CTCF protein levels in wildtype and Snf2h ko cells (lamin B is shown as a loading control, for gel source data, see Supplementary Figure 1). **h,i,** Average CpG methylation around bound CTCF motifs (h) and REST motifs (i) in wildtype and Snf2h ko cells. **j,** Profiles of MNase and de-trended methylation data downstream of REST motifs, with indicated nucleosome positions and offsets between wildtype and Snf2h ko. Profiles illustrate high MNase signal at phased nucleosomes, and high methylation values in the respective linker regions. The shift between wildtype and Snf2h ko maximal signals in the third peak is indicated by black lines.

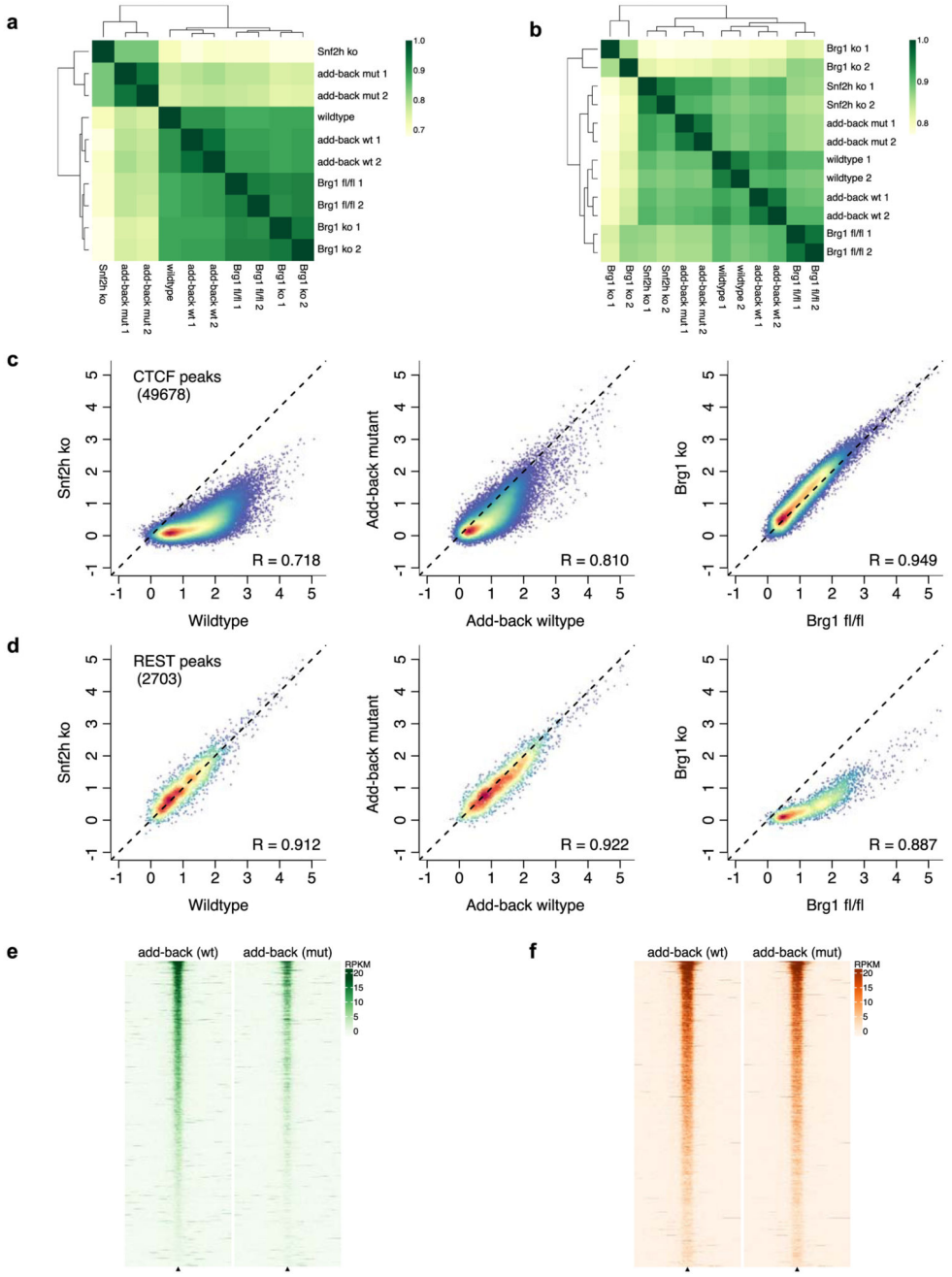

Extended Data Figure 9. Genome-wide binding of CTCF and REST in Snf2h ko, add-back clones, Brg1 ko and wt cells.

a,b, Unsupervised clustering of ChIP enrichments (log2 IP/input) in motif-containing CTCF peaks (a, n=49,678) and REST peaks (b, n=2,703) for individual biological replicates from cells with different Snf2h and Brg1 genotypes. The colours between white and green indicate Pearson's correlation coefficient between pairs of samples. **c**, CTCF ChIP enrichments (log2 IP/input) for motif containing CTCF peaks. The panels compare transcription factor binding in wildtype and Snf2 ko (left), wildtype and mutant add-backs

Europe PMC Funders Author Manuscripts

(middle) and Brg1 fl/fl to Brg1 ko cells (right). R: Pearson's correlation coefficient. **d**, Same as in (c) for REST. **e,f,** ChIP seq alignment density in Snf2h add-back cells +/- 1kb around random sets of 2000 ChIP peaks for CTCF (e) and REST (f). The arrow at the bottom indicates the location of the predicted TF binding site.

Europe PMC Funders Author Manuscripts

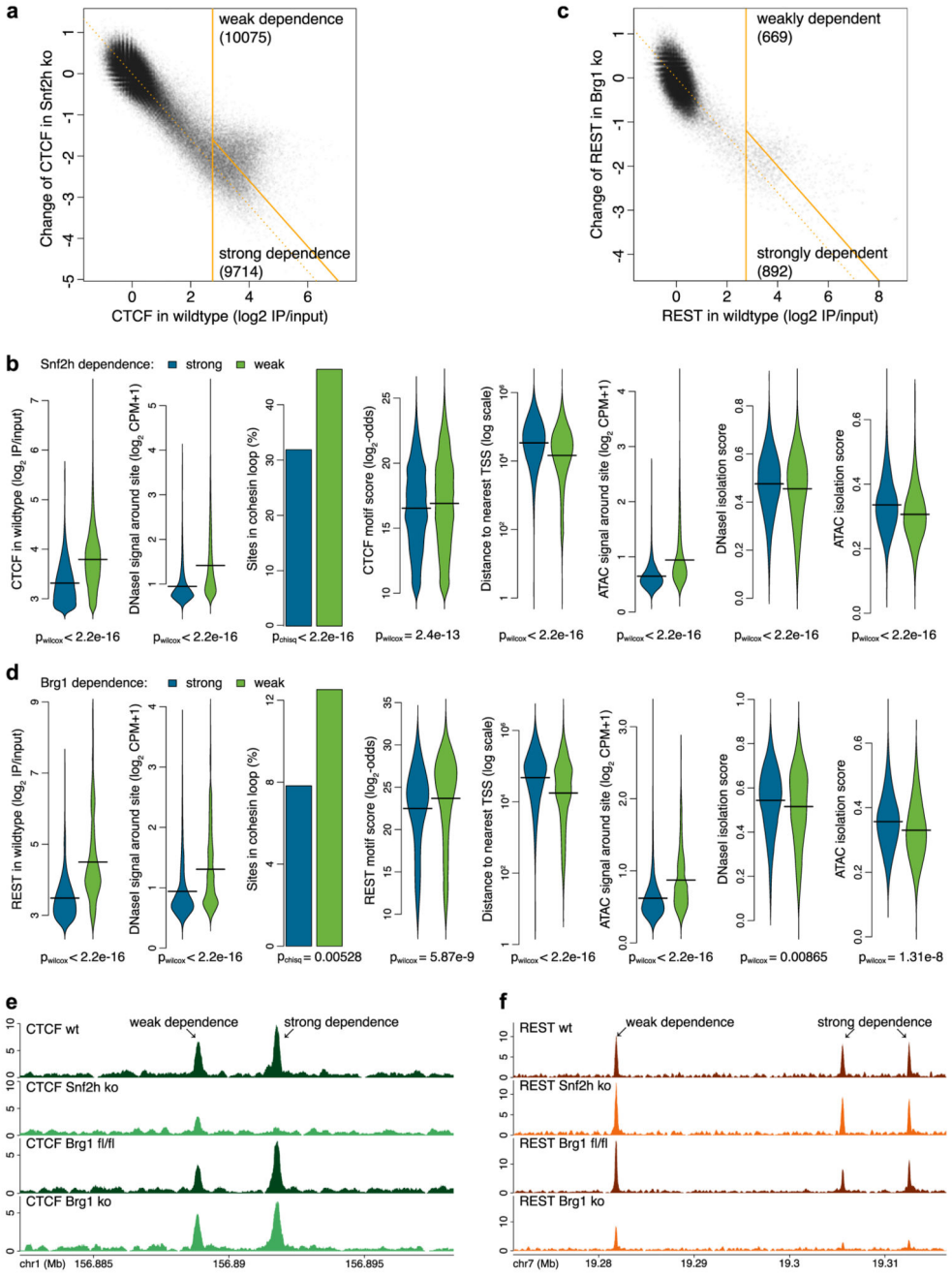

Extended Data Figure 10. Comparison of CTCF and REST binding sites with variable dependencies on specific chromatin remodellers.

a, Wildtype CTCF binding (x-axis) and change of binding between Snf2h ko and wildtype (y-axis) at predicted CTCF motifs. Strongly bound motifs can be sub-divided into sites with strong and weak dependence on Snf2h, based on their loss of CTCF binding upon Snf2h knockout. **b**, Comparison of strongly and weakly dependent sites in terms of wildtype CTCF enrichment, accessibility in the neighbourhood measured by DNase I, frequency of sites that are part of cohesin chromatin loops (Mumbach et al. 2016), CTCF motif score, distance to

nearest TSS, accessibility in the close neighbourhood measured by ATAC and isolation score (fraction of DNAse I or ATAC signal in central 200bp versus 2kb). **c,d**, Same as in (a),(b) for REST. **e,f,** Two exemplary loci with CTCF (e) and REST (f) ChIP tracks in cells of different Snf2h and Brg1 genotypes (rpkm in 5bp bins). Weakly and strongly dependent binding sites are indicated.

Europe PMC Funders Author Manuscripts

Europe PMC Funders Author Manuscripts

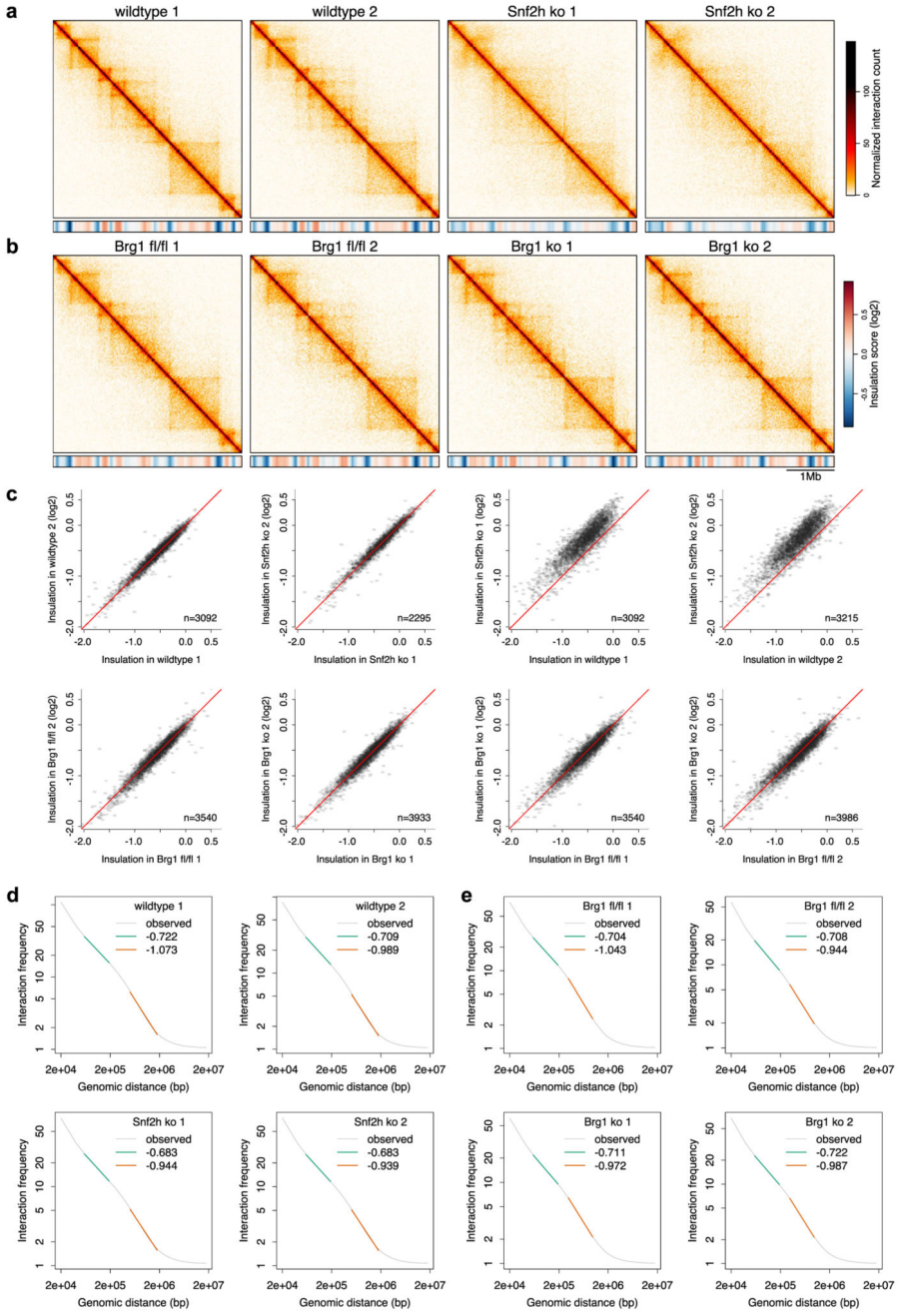

Extended Data Figure 11. Measurements of chromatin conformation by Hi-C in individual replicates.

a,b, Normalized Hi-C contact maps at 20kb resolution for individual replicates for a representative 4Mb region on chromosome 16 (25-29Mb), from cells with different Snf2h (a) or Brg1 (b) genotypes. Insulation scores for 200kb squares are shown at the bottom as a heatmap. **c,** Insulation scores (200kb squares) for TAD boundaries with CTCF binding sites detected in individual replicates of Snf2h and Brg1 deleted cells with corresponding wildtype controls. **d,e** Log interaction frequency as a function of log distance for individual

Hi-C replicates in Snf2h wildtype and knockout cells (d) and Brg1 fl/fl and knockout cells (e). The decay exponents have been estimated for short (50-200kb) and long genomic distances (0.5-2Mb in c and 0.3-1Mb in d), omitting the non-linear part at the bottom.

Europe PMC Funders Author Manuscripts

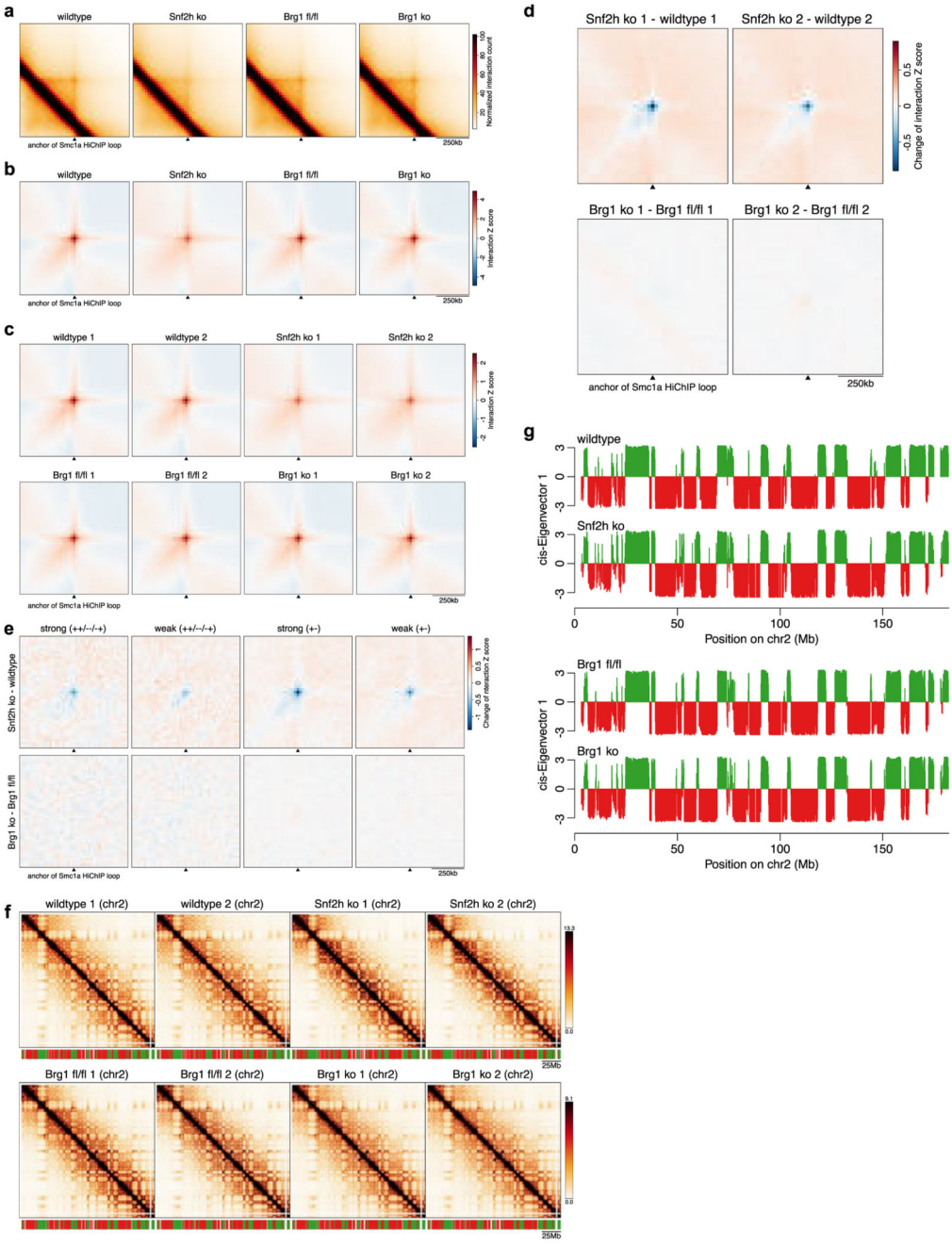

Extended Data Figure 12. CTCF-cohesin loops and A/B compartments in individual replicates.

a, Interaction frequencies at Smc1a HiChip loops, aggregated over loops separated by 280 to 380kb (n=701). **b,** Interaction Z scores at Smc1a HiChip loops, aggregated over loops separated by 60 to 500kb (n=4,375) and averaged over two biological replicates. **c,** Same as in (b) for individual replicates. **d,** Changes of interaction Z scores at Smc1a HiChip loops from (c) in individual replicate pairs. **e,** Changes of interaction Z scores at Smc1a HiChip loops, separated by CTCF motif orientation (+-: convergent, ++/-- /-+: other) and dependency on Snf2h (strong or weak). **f,** Normalized Hi-C contact maps at 150kb

Europe PMC Funders Author Manuscripts

resolution for entire chromosome 2 showing individual replicates. A/B compartments are indicated below in green and red, respectively. **g,** cis-Eigenvector 1 values (multiplied by 100) across entire chromosome 2.

Supplementary Material

Refer to Web version on PubMed Central for supplementary material.

Acknowledgements

We would like to thank Luca Giorgetti and Lukas Burger for suggestions and feedback, Christiane Wirbelauer for technical assistance, Sebastien Smallwood for next-generation sequencing support and members of the Schübeler group for feedback on project and manuscript. Brg1 fl/fl ES cells were kindly provided by Jerry Crabtree (Stanford University). Research in the laboratory of D.S. is supported by the Novartis Research Foundation, the European Research Council (ERC) under the European Union's Horizon research and innovation program (Grant agreement no. 667951) and the Swiss National Sciences Foundation. D.B. was funded by a Boehringer Ingelheim Fonds PhD fellowship. M.I. is funded by an EMBO Long-term postdoctoral fellowship.

References

1. Becker PB, Hörz W. ATP-dependent nucleosome remodeling. Annu Rev Biochem. 2002; 71:247–273. [PubMed: 12045097]
2. Clapier CR, Cairns BR. The Biology of Chromatin Remodeling Complexes. Annu Rev Biochem. 2009; 78:273–304. [PubMed: 19355820]
3. Kadoch C, Crabtree GR. Mammalian SWI/SNF chromatin remodeling complexes and cancer: Mechanistic insights gained from human genomics. Sci Adv. 2015; 1:e1500447–e1500447. [PubMed: 26601204]
4. Ho L, et al. esBAF facilitates pluripotency by conditioning the genome for LIF/STAT3 signalling and by regulating polycomb function. Nat Cell Biol. 2011; 13:903–913. [PubMed: 21785422]
5. Ho L, Crabtree GR. Chromatin remodelling during development. Nature. 2010; 463:474–484. [PubMed: 20110991]
6. Miller EL, et al. TOP2 synergizes with BAF chromatin remodeling for both resolution and formation of facultative heterochromatin. Nat Struct Mol Biol. 2017; 24:344–352. [PubMed: 28250416]
7. King HW, Klose RJ. The pioneer factor OCT4 requires the chromatin remodeller BRG1 to support gene regulatory element function in mouse embryonic stem cells. Elife. 2017; 6:380.
8. Fry CJ, Peterson CL. Chromatin remodeling enzymes: who's on first? Current biology: CB. 2001; 11:R185–97. [PubMed: 11267889]
9. Vignali M, Hassan AH, Neely KE, Workman JL. ATP-dependent chromatin-remodeling complexes. Molecular and cellular biology. 2000; 20:1899–1910. [PubMed: 10688638]
10. Corona DFV, Tamkun JW. Multiple roles for ISWI in transcription, chromosome organization and DNA replication. Biochimica et biophysica acta. 2004; 1677:113–119. [PubMed: 15020052]
11. Deuring R, et al. The ISWI chromatin-remodeling protein is required for gene expression and the maintenance of higher order chromatin structure in vivo. Molecular cell. 2000; 5:355–365. [PubMed: 10882076]
12. Yen K, Vinayachandran V, Batta K, Koerber RT, Pugh BF. Genome-wide nucleosome specificity and directionality of chromatin remodelers. Cell. 2012; 149:1461–1473. [PubMed: 22726434]
13. Längst G, Becker PB. Nucleosome mobilization and positioning by ISWI-containing chromatin-remodeling factors. Journal of cell science. 2001; 114:2561–2568. [PubMed: 11683384]
14. Yamada K, et al. Structure and mechanism of the chromatin remodelling factor ISW1a. Nature. 2011; 472:448–453. [PubMed: 21525927]
15. Ocampo J, Chereji RV, Eriksson PR, Clark DJ. The ISW1 and CHD1 ATP-dependent chromatin remodelers compete to set nucleosome spacing in vivo. Nucleic acids research. 2016; 44:4625–4635. [PubMed: 26861626]

16. Wiechens N, et al. The Chromatin Remodelling Enzymes SNF2H and SNF2L Position Nucleosomes adjacent to CTCF and Other Transcription Factors. PLoS Genet. 2016; 12:e1005940. [PubMed: 27019336]
17. Stopka T, Skoultchi AI. The ISWI ATPase Snf2h is required for early mouse development. Proceedings of the National Academy of Sciences. 2011; 100:14097–14102.
18. Hakimi M-A, et al. A chromatin remodelling complex that loads cohesin onto human chromosomes. Nature. 2002; 418:994–998. [PubMed: 12198550]
19. Oppikofer M, et al. Expansion of the ISWI chromatin remodeler family with new active complexes. EMBO Rep. 2017; 18:1697–1706. [PubMed: 28801535]
20. Gkikopoulos T, et al. A role for Snf2-related nucleosome-spacing enzymes in genome-wide nucleosome organization. Science. 2011; 333:1758–1760. [PubMed: 21940898]
21. Kelly TK, et al. Genome-wide mapping of nucleosome positioning and DNA methylation within individual DNA molecules. Genome research. 2012; 22:2497–2506. [PubMed: 22960375]
22. Buenrostro JD, Giresi PG, Zaba LC, Chang HY, Greenleaf WJ. Transposition of native chromatin for fast and sensitive epigenomic profiling of open chromatin, DNA-binding proteins and nucleosome position. Nat Methods. 2013; 10:1213–1218. [PubMed: 24097267]
23. Ho L, et al. An embryonic stem cell chromatin remodeling complex, esBAF, is essential for embryonic stem cell self-renewal and pluripotency. Proceedings of the National Academy of Sciences of the United States of America. 2009; 106:5181–5186. [PubMed: 19279220]
24. Valouev A, et al. Determinants of nucleosome organization in primary human cells. Nature. 2011; 474:516–520. [PubMed: 21602827]
25. Teif VB, et al. Genome-wide nucleosome positioning during embryonic stem cell development. Nat Struct Mol Biol. 2012; 19:1185–1192. [PubMed: 23085715]
26. Mathelier A, et al. JASPAR 2016: a major expansion and update of the open-access database of transcription factor binding profiles. Nucleic acids research. 2016; 44:D110–5. [PubMed: 26531826]
27. Stadler MB, et al. DNA-binding factors shape the mouse methylome at distal regulatory regions. Nature. 2011; 480:490–495. [PubMed: 22170606]
28. Lambert SA, et al. The Human Transcription Factors. Cell. 2018; 172:650–665. [PubMed: 29425488]
29. Dekker J, Mirny L. The 3D Genome as Moderator of Chromosomal Communication. Cell. 2016; 164:1110–1121. [PubMed: 26967279]
30. Merkenschlager M, Nora EP. CTCF and Cohesin in Genome Folding and Transcriptional Gene Regulation. Annu Rev Genomics Hum Genet. 2016; 17:17–43. [PubMed: 27089971]
31. Nora EP, et al. Targeted Degradation of CTCF Decouples Local Insulation of Chromosome Domains from Genomic Compartmentalization. Cell. 2017; 169:930–944.e22. [PubMed: 28525758]
32. Crane E, et al. Condensin-driven remodelling of X chromosome topology during dosage compensation. Nature. 2015; 523:240–244. [PubMed: 26030525]
33. Mumbach MR, et al. HiChIP: efficient and sensitive analysis of protein-directed genome architecture. Nat Methods. 2016; 13:919–922. [PubMed: 27643841]
34. Lieberman-Aiden E, et al. Comprehensive mapping of long-range interactions reveals folding principles of the human genome. Science. 2009; 326:289–293. [PubMed: 19815776]
35. Fyodorov DV, Blower MD, Karpen GH, Kadonaga JT. Acf1 confers unique activities to ACF/CHRAC and promotes the formation rather than disruption of chromatin in vivo. Genes & development. 2004; 18:170–183. [PubMed: 14752009]

Europe PMC Funders Author Manuscripts

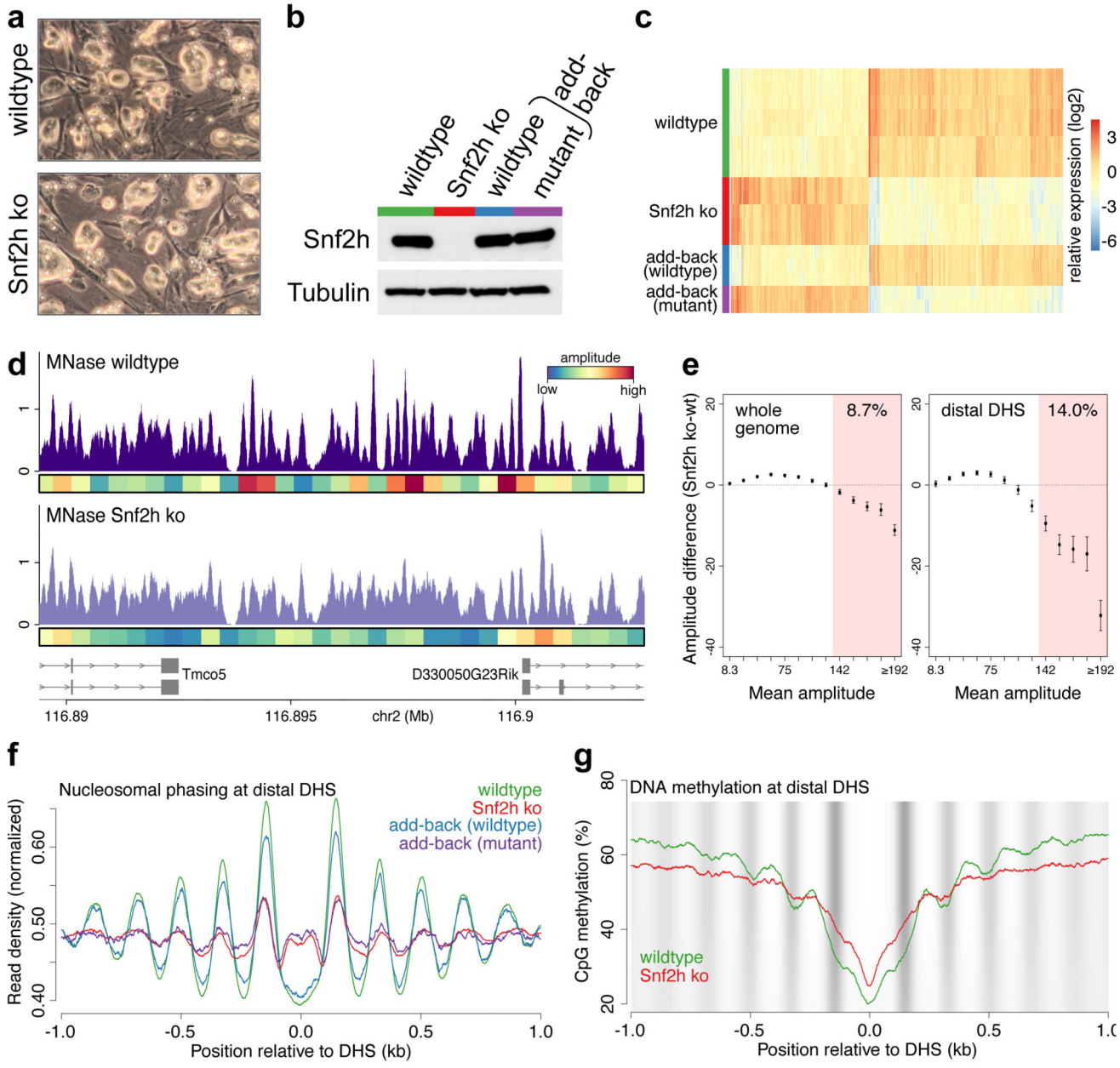

Figure 1. Deletion of Snf2h in mouse embryonic stem cells causes genome-wide reduction in nucleosome phasing.

a, Wildtype and Snf2h ko mouse stem cell cultures. **b,** Western blot detecting Snf2h protein levels in wildtype, ko and add-back cells. Tubulin is used as loading control (for gel source data, see Supplementary Figure 1). **c,** Heatmap of relative expression (log2 fold-change relative to the mean over all samples) for all differentially expressed genes between any pair of conditions (1,107 genes with FDR < 0.001 and fold-change greater than 3). **d,** Locus on chromosome 2 showing MNase-seq read densities and amplitude values for nucleosomal frequency. **e,** Amplitude differences between Snf2h ko and wildtype cells, stratified by mean amplitude, for whole genome (left) and distal (>1kb from TSSs) DNase I hypersensitive

sites (DHS) (right). Percentage of regions with high amplitudes (red shaded area, top 5 bins) is indicated. **f,** Average MNase-seq read densities around distal DHS. **g,** Average CpG methylation around distal DHS. Nucleosomes are illustrated in grey in the background (MNase signal from (f).

Europe PMC Funders Author Manuscripts

Europe PMC Funders Author Manuscripts

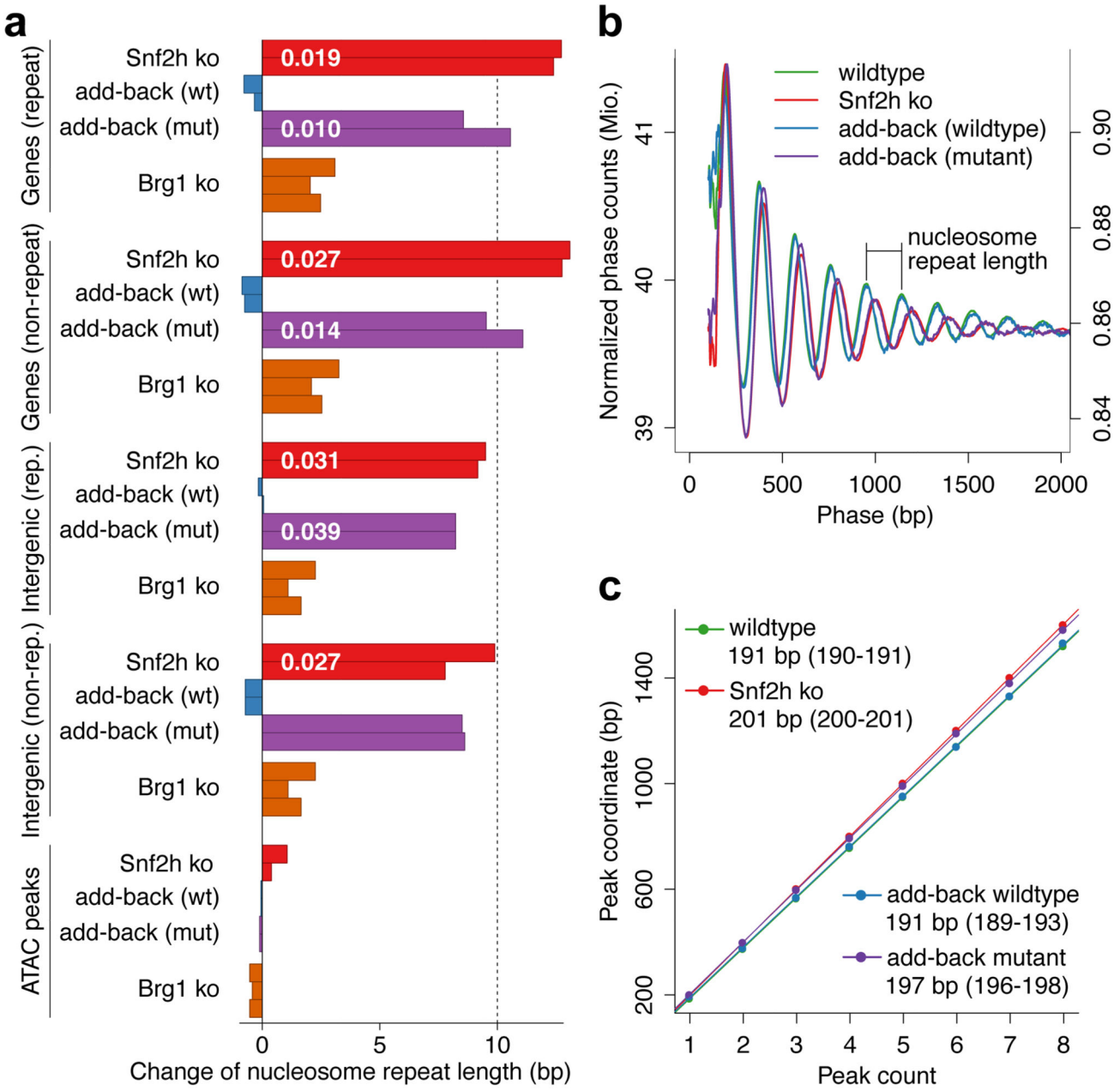

Figure 2. Loss of Snf2h increases nucleosome repeat length.

a, Changes in nucleosome repeat lengths (NRLs) based on ATAC-seq data in different Snf2h and Brg1 genotypes compared to wildtype/controls. P values for a one-sided Welch two sample t-test are shown ($p > 0.05$ if not shown). **b,c,** MNase-based estimation of NRL. b) Counts of distances between same-strand MNase-seq alignments (phase) in wildtype, Snf2h ko and add-back cells (add-backs are on the right y-axis). c) Linear fits to the phase peaks from (b) and resulting NRLs with 95% confidence intervals.

Europe PMC Funders Author Manuscripts

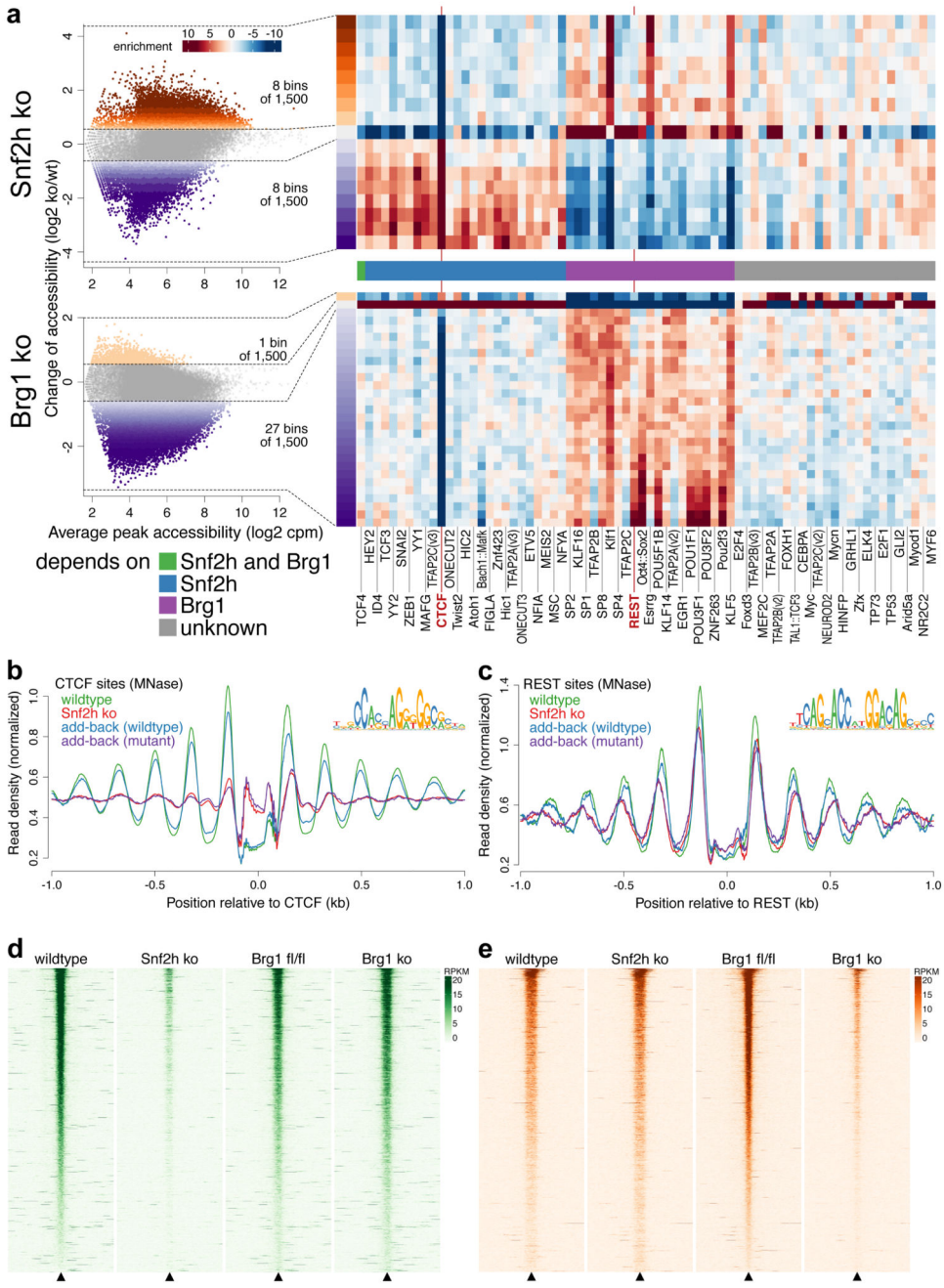

Figure 3. Selective dependence on Snf2h or Brg1 defines subsets of mammalian transcription factors.

a, Comprehensive computational screen of 519 mammalian transcription factors with known binding motifs regarding their dependency on Snf2h or Brg1. Enrichments of predicted TF binding sites were calculated in ATAC-seq peaks binned according to change of accessibility in Snf2h or Brg1 ko. **b,c,** MNase profiles for exemplary transcription factors CTCF and REST with differing dependency on Snf2h or Brg1 in wildtype and Snf2h ko cells. **d,e,** ChIP

seq alignment density +/- 1kb around random sets of 2000 ChIP peaks for CTCF (f) and REST (g). Center indicates location of predicted TF binding site.

Europe PMC Funders Author Manuscripts

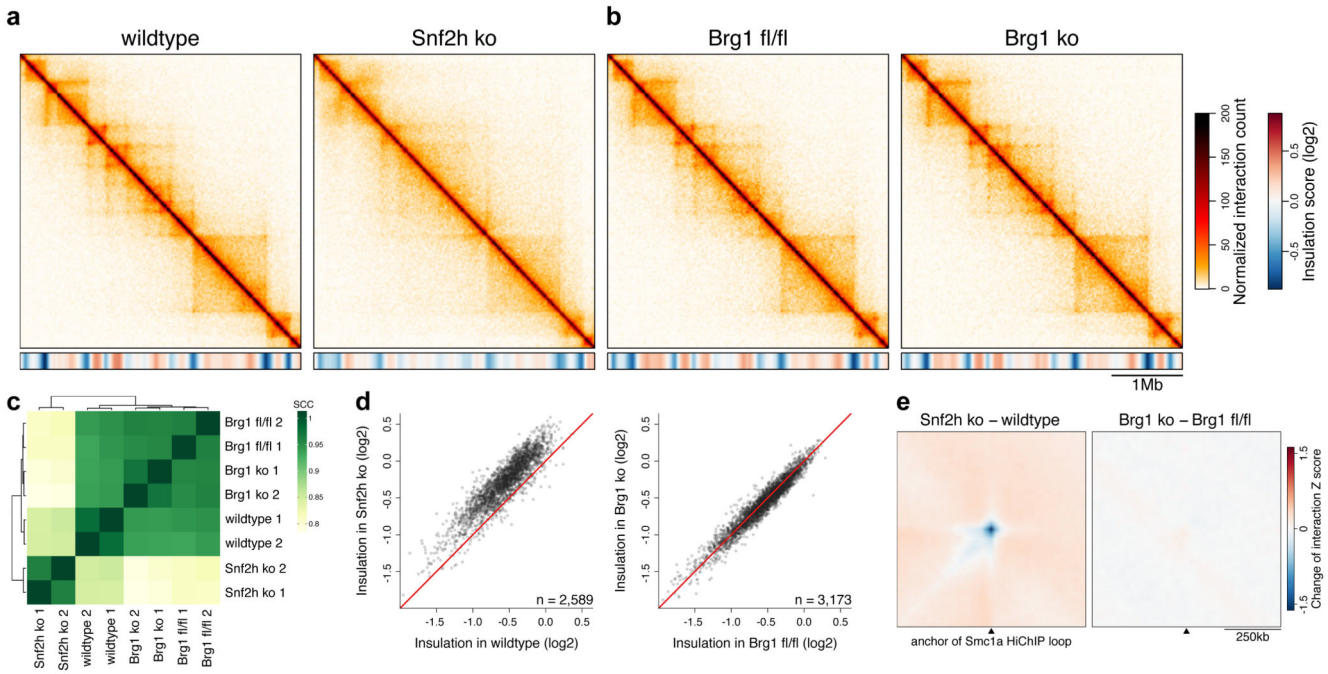

Figure 4. Loss of Snf2h but not Brg1 affects chromosome conformation.

a,b, Normalized Hi-C contact maps at 20kb resolution for a representative 4Mb region on chromosome 16 (25-29Mb), from cells with different Snf2h (a) or Brg1 (b) genotypes. Insulation scores for 200kb squares are shown at the bottom as a heatmap. **c,** Unbiased clustering of Hi-C contact matrices (chromosome 10 at 20kb resolution). Colors indicate pairwise stratum-adjusted correlation coefficients (SCC, higher values correspond to higher similarity). **d,** Insulation scores (200kb squares) for TAD boundaries with CTCF binding sites detected in wildtype (left) and Brg1 fl/fl cells (right), compared to the insulation in the respective knockout cells. **e,** Changes of interaction Z scores at Smc1a HiChip loops, aggregated over loops separated by 60 and 500 kb (n=4,375).

Europe PMC Funders Author Manuscripts